Positron flight in human tissues and its influence on PET image spatial resolution

Alejandro Sánchez-Crespo[1, 2], Pedro Andreo[2], Stig A. Larsson[1, 2]

[1] Section of Nuclear Medicine, Department of Hospital Physics, Karolinska Hospital, Stockholm, Sweden
[2] Medical Radiation Physics, Department of Oncology-Pathology, Stockholm University and Karolinska Institute, Stockholm, Sweden

Published online: 10 October 2003

Abstract. The influence of the positron distance of flight in various human tissues on the spatial resolution in positron emission tomography (PET) was assessed for positrons from carbon-11, nitrogen-13, oxygen-15, fluorine-18, gallium-68 and rubidium-82. The investigation was performed using the Monte Carlo code PENELOPE to simulate the transport of positrons within human compact bone, adipose, soft and lung tissue. The simulations yielded 3D distributions of annihilation origins that were projected on the image plane in order to assess their impact on PET spatial resolution. The distributions obtained were cusp-shaped with long tails rather than Gaussian shaped, thus making conventional full width at half maximum (FWHM) measures uncertain. The full width at 20% of the maximum amplitude (FW20M) of the annihilation distributions yielded more appropriate values for root mean square addition of spatial resolution loss components. Large differences in spatial resolution losses due to the positron flight in various human tissues were found for the selected radionuclides. The contribution to image blur was found to be up to three times larger in lung tissue than in soft tissue or fat and five times larger than in bone tissue. For ^{18}F, the spatial resolution losses were 0.54 mm in soft tissue and 1.52 mm in lung tissue, compared with 4.10 and 10.5 mm, respectively, for ^{82}Rb. With lung tissue as a possible exception, the image blur due to the positron flight in all human tissues has a minor impact as long as PET cameras with a spatial resolution of 5–7 mm are used in combination with ^{18}F-labelled radiopharmaceuticals. However, when ultra-high spatial resolution PET cameras, with 3–4 mm spatial resolution, are applied, especially in combination with other radionuclides, the positron flight may enter as a limiting factor for the total PET spatial resolution—particularly in lung tissue.

Alejandro Sánchez-Crespo (✉)
Section of Nuclear Medicine, Department of Hospital Physics,
Karolinska Hospital, 176 76 Stockholm, Sweden
e-mail: alejandro.sanchez-crespo@ks.se
Tel.: +46-8-51779315, Fax: +46-8-51774939

Keywords: Positron range – Spatial resolution – Annihilation – PET – Point spread function

Eur J Nucl Med Mol Imaging (2004) 31:44–51
DOI 10.1007/s00259-003-1330-y

Introduction

Major factors influencing positron emission tomography (PET) spatial resolution are the positron range, the non-colinearity of annihilating photons, the intrinsic properties, the size and geometry of the detector and the selection of the reconstruction algorithm. In practice, patient movements during long acquisition sequences also contribute to the image blur. Aspects of the detector design and physical properties and their influence on system spatial resolution have been extensively addressed by many authors, leading to a continuous optimisation of hardware [1, 2, 3, 4, 5, 6]. The impact of the positron flight (which does not represent the positron continuous slowing-down range, a tortuous path due to multiple scattering, but the linear distance from the positron source to the annihilation point) on spatial resolution has also been analysed. This has been done experimentally [7, 8], through theoretical calculations based on an empirical range formula [9] or by Monte Carlo calculations [10]. These studies share the same limitation of having been performed using water as the reference medium for positron interaction. Surprisingly enough, values reported in the literature show large discrepancies in the full width at half maximum (FWHM) of the projected positron flight around the source. Furthermore, the exclusive use of data in water for clinical practice can be rather misleading since positron interactions with matter are influenced by both atomic composition and tissue density. Thus, it is expected that the cloud of annihilation points around the positron source will vary in size and shape depending on the kind of tissue in which the positron transport takes place. In order to assess the

effect of the positron distance of flight on the image-plane spatial resolution in clinical PET imaging, therefore, the positron transport should be modelled separately for each specific tissue. Such a detailed analysis may be especially considered for high spatial resolution PET applications. The aim of this paper was to assess the positron flight contribution to spatial resolution losses in PET imaging for some common positron emission sources in various human tissues using the Monte Carlo method.

Materials and methods

Principle of the method. The PENELOPE Monte Carlo system [11, 12, 13] was used to simulate the transport of positrons and their cascade of interactions in human compact bone (1.85 g cm^{-3}), adipose tissue (0.92 g cm^{-3}), soft tissue (1.00 g cm^{-3}) and lung tissue (0.30 g cm^{-3}). The different compositions for these human tissues were obtained from ICRU [14] and ICRP [15].

Mono-energetic point isotropic positron sources in the energy range from 25 keV to 3,325 keV, with a 25-keV sampling grid, were situated at the origin of coordinates centered in a sphere of homogeneous tissue T_j, with defined density ρ_j and a radius much longer than the expected positron continuous slowing down range in that medium. The transport of individual positrons with initial kinetic energy E_i was simulated with a sampling positron interaction step-length of 0.1 mm down to a cut-off energy of 1 keV. Below this energy, the positron was assumed to form positronium and annihilate. The probability for in-flight annihilation was also included in the simulation process.

Given a radioactive point source emitting positrons with initial kinetic energy E_i in tissue T_j, the generated Cartesian coordinates of each annihilation event were registered in a phase-space file, representing the 3D annihilation point spread function $aPSF(T_j,E_i,x,y,z)$. This process yielded a database of functions for each tissue and for each mono-energetic isotropic positron emitter source. From this database, the corresponding annihilation point spread functions for the positron spectra of carbon-11, nitrogen-13, oxygen-15, fluorine-18, gallium-68 and rubidium-82 in different human tissues, $aPSF(T_j,{}_zX^A,x,y,z)$, were obtained as the weighted sum of the obtained discrete annihilation distributions, according to:

$$aPSF(T_j,{}_zX^A,x,y,z)=\sum_i^S aPSF(T_j,E_i,x,y,z)\cdot W_i({}_zX^A,E_i) \qquad (1)$$

where the weighting factors $W_i({}_zX^A,E_i)$ represent the positron decay probability with energy E_i for the radionuclide ${}_zX^A$, as obtained from tabulated probability disintegration schemes [16; Stephen M. Seltzer (National Institute of Standards and Technology, Gaithersburg, USA), personal communications]. The sum of the weighting factors was normalised to unity.

For assessment of the spatial distribution functions at the detector level, the 3D volume of annihilation origins around each radionuclide point source was projected onto a perpendicular plane by sampling $aPSF(T_j,{}_zX^A,x,y,z)$ along an arbitrary direction. The obtained image-plane annihilation point spread function $aPSF(T_j,{}_zX^A,x)$ represents the one-dimensional probability distribution function for positron annihilation around a point source of radionuclide ${}_zX^A$ within a tissue T_j.

Influence of the positron flight on PET spatial resolution. The relative influence of the positron flight on the total PET spatial resolution depends on the system spatial resolution of the camera. This includes the intrinsic camera properties, the detector geometry-dependent non-colinearity of annihilation photons and the parallax errors due to various depths of interaction in the detector. These factors were included in the analysis by convolving $aPSF(T_j,{}_zX^A,x)$ with a Gaussian function representing the PET system spatial resolution in the x-direction. The relative spatial resolution loss due to the positron range was assessed in percent of the system spatial resolution according to:

$$\Delta(T_{j,Z}X^A)(\%)=\left(\frac{FWHM(T_{j,Z}X^A)_{Convolved}}{FWHM_{System}}-1\right)\cdot 100 \qquad (2)$$

where $FWHM(T_{j,Z}X^A)_{Convolved}$ and $FWHM_{System}$ respectively represent the full width at half maximum of the convolved data set and the PET system spatial resolution.

$FWHM(T_{j,Z}X^A)_{Convolved}$ represents the most probable estimator of the total PET spatial resolution including both the camera resolution and the positron range distributions. A more simple spatial resolution estimator, commonly used for approximating the total spatial resolution, may be obtained by calculating the root mean square of the individual resolution components, according to:

$$FWHM(T_{j,Z}X^A)_{Total}=\sqrt{FWHM^2_{System}+B(T_{j,Z}X^A)^2} \qquad (3)$$

where $FWHM(T_j,\ X_A)_{Total}$ represents the total PET spatial resolution. The parameter B is a measure of the image blur due to the positron flight distribution. In order to analyse the accuracy of the approximation given by Eq 3, as compared to direct convolution, two alternative B values were selected and applied in combination with a system spatial resolution of 3 mm. The selected B values were, respectively, the FWHM (full width at half maximum) and FW20M (full width at twentieth maximum).

Stability of the calculated annihilation point spread functions to energy rebinding effects. In bone, adipose and soft tissue, energy rebinding effects in the resulting annihilation point spread functions could be of little significance due to the very limited positron distance of flight for similar positron energies. In contrast, in lung tissue, where the positron flight is much larger, the results could depend on the selected energy sampling grid. Hence, $aPSF(T_j,{}_zX^A,x)$ were calculated using an energy sampling interval of 50 keV and the corresponding $FWHM(T_{j,Z}X^A)_{aPSF}$ and $FWTM(T_{j,Z}X^A)_{aPSF}$ values were compared with those obtained with a narrow 25-keV sampling interval.

Results

The large differences in image blur due to the positron flight in human compact bone, soft tissue and lung tissue from some characteristic positron point sources are illustrated in Fig. 1. The corresponding one-dimensional annihilation probability distribution functions $aPSF({}_zX^A,T_i,x)$, as a function of distance from the point source, are presented in Fig. 2 for each radionuclide and for each of the selected tissues. All projected distributions of annihilation events were cusp shaped around the

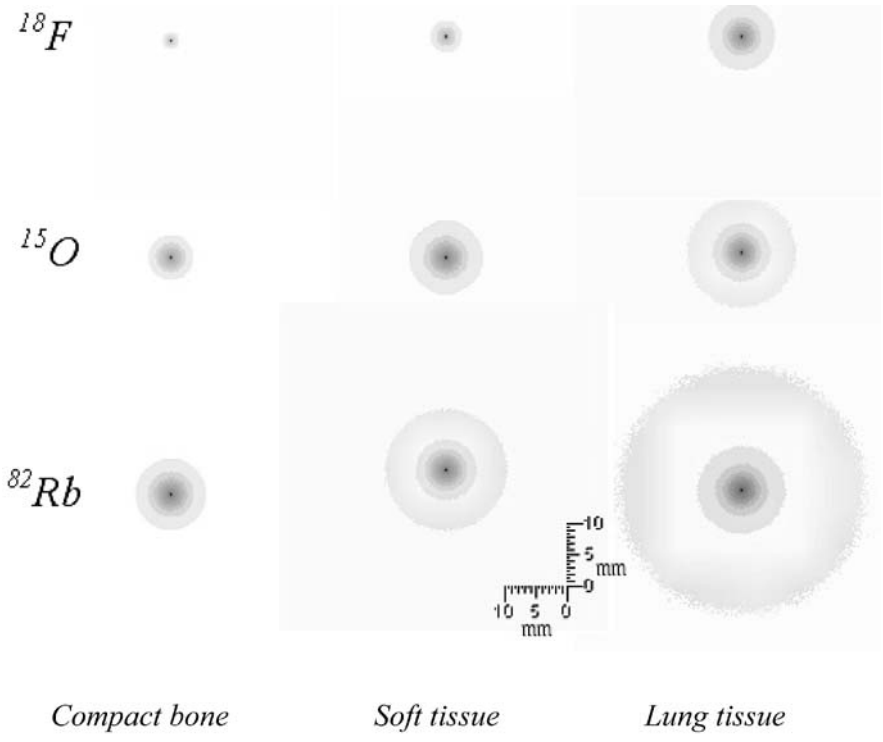

Fig. 1. Monte Carlo-calculated distribution of annihilation events around a positron point source embedded in different human tissues as seen in the image plane of a PET camera

Table 1. Three alternative measures, FWHM, FW20M and FWTM, for assessing the spatial resolution loss due to the tissue- and radionuclide-dependent positron annihilation point spread functions

Radionuclide	Compact bone			Soft tissue			Adipose tissue			Lung tissue		
	FWHM (mm)	FW20M (mm)	FWTM (mm)	FWHM (mm)	FW20M (mm)	FWTM (mm)	FWHM (mm)	FW20M (mm)	FWTM (mm)	FWHM (mm)	FW20M (mm)	FWTM (mm)
^{18}F	0.18	0.42	0.65	0.19	0.54	0.91	0.19	0.58	0.97	0.37	1.52	2.70
^{11}C	0.22	0.62	0.92	0.28	0.96	1.70	0.30	1.15	2.09	0.52	2.69	4.90
^{13}N	0.26	0.72	1.14	0.33	1.26	2.12	0.37	1.55	2.70	0.62	3.50	6.50
^{15}O	0.33	1.08	1.90	0.41	1.87	3.10	0.50	2.31	3.90	0.86	5.30	10.10
^{68}Ga	0.36	1.29	2.30	0.49	2.12	3.70	0.57	2.67	4.30	0.98	6.10	11.50
^{82}Rb	0.56	2.68	4.50	0.76	4.10	7.60	0.81	4.30	7.70	1.43	10.50	20.30

positron point source. Due to this characteristic shape, all related FWHM values were well within the system resolution of a modern PET camera (4–5 mm). The corresponding $FWTM(T_{j,Z}X^A)_{aPSF}$ values, on the other hand, varied from 0.65 mm in bone up to 2.7 mm in lung tissue for ^{18}F and from 4.5 mm in bone up to 20.3 mm in lung tissue for ^{82}Rb. This is illustrated in Table 1 together with the values at the 20% level, $FW20M(T_{j,Z}X^A)_{aPSF}$.

The properties of the positron annihilation distributions are further illustrated in Table 2, which shows the fraction of events within the selected widths of $aPSF({}_zX^A, T_i, x)$. The fractions decrease with decreasing tissue density and increasing positron energy. This may be due to the different energy-dependent scatter properties of the considered media and their influence on the positron transport mechanisms. Furthermore, the fractions obtained within the selected levels of Table 2 are in clear contrast to those obtained for a standardised Gaussian distribution, normally taken as an estimator of the system spatial resolution, where the corresponding constant fractions for the FWHM and the FWTM are respectively 76% and 97%.

The impact of the positron distance of flight on total spatial resolution is illustrated in Fig. 3 as a function of the system spatial resolution. These curves show the positron annihilation point spread distribution convolved with Gaussian functions, representing various spatial resolution of the PET camera. The disturbing image blur caused by the positron flight becomes increasingly important when aiming at high-resolution PET cameras, with a system spatial resolution below 5 mm FWHM. The higher the system spatial resolution, the higher is the

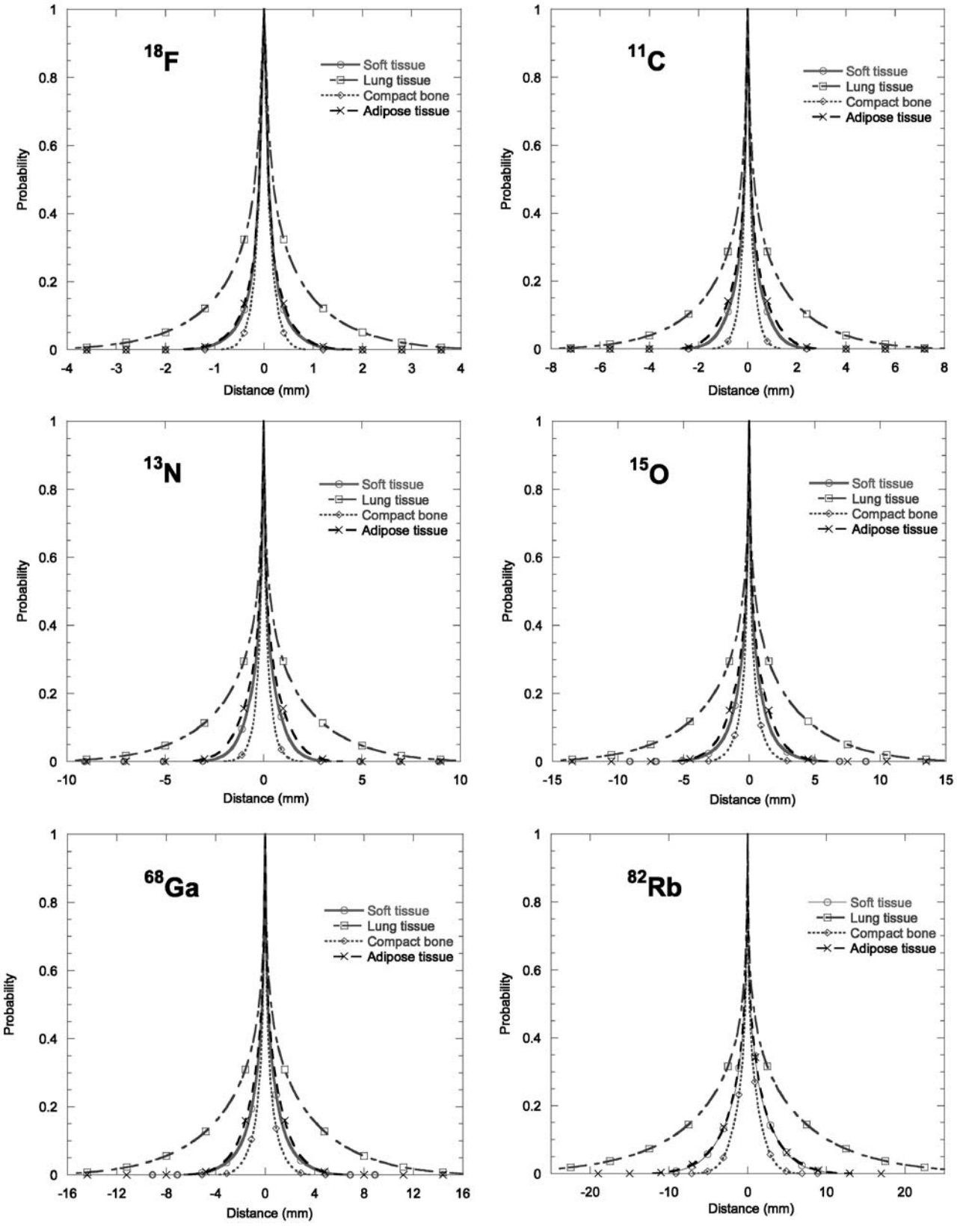

Fig. 2. Projected annihilation point spread probability distributions $aPSF({}_zX^A, T_i, x)$ normalised to 1.0 at zero distance

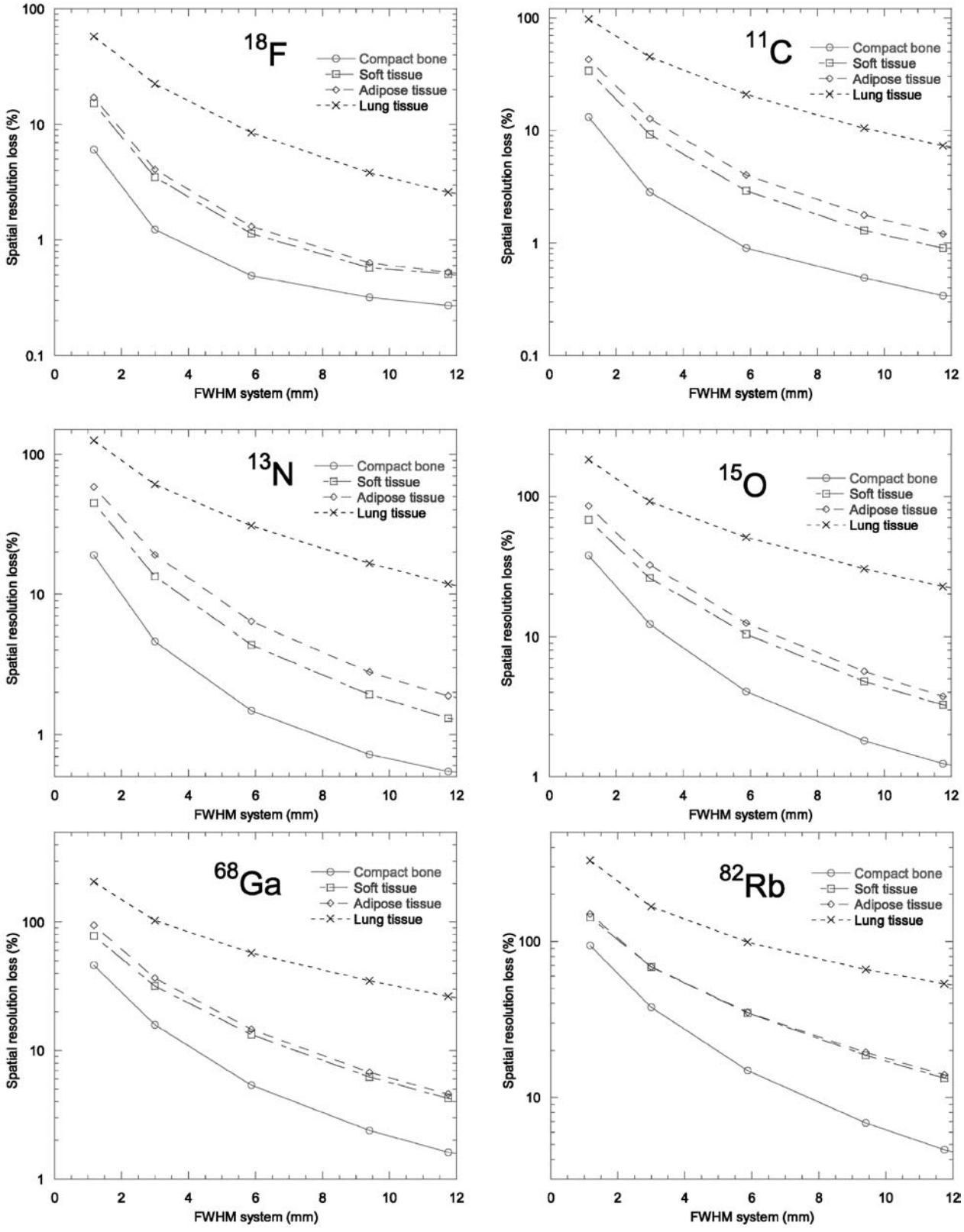

Fig. 3. Relative spatial resolution loss (%) due to the positron distance of flight in various human tissues as a function of the system spatial resolution (FWHM) of the PET camera

Table 2. Relative fraction of events within the FWHM, the FW20M and the FWTM levels of the projected $aPSF({}_zX^A, T_i, x)$

Radio-nuclide	Compact bone			Soft tissue			Adipose tissue			Lung tissue		
	FWHM (mm)	FW20M (mm)	FWTM (mm)	FWHM (mm)	FW20M (mm)	FWTM (mm)	FWHM (mm)	FW20M (mm)	FWTM (mm)	FWHM (mm)	FW20M (mm)	FWTM (mm)
^{18}F	49.8	79.0	89.7	39.3	69.9	84.2	37.1	68.9	84.1	26.5	63.3	81.8
^{11}C	43.0	75.2	87.9	32.7	67.6	85.4	29.9	66.7	84.9	21.5	60.9	80.8
^{13}N	40.3	72.9	86.1	30.5	68.3	85.3	27.5	68.0	85.8	19.4	60.1	80.6
^{15}O	33.3	67.0	82.9	25.6	65.5	82.2	25.4	68.2	85.0	17.1	59.3	80.4
^{68}Ga	31.4	66.4	83.5	25.4	65.1	82.0	25.3	68.4	83.5	17.1	60.1	80.9
^{82}Rb	25.4	67.9	85.9	20.4	62.2	82.7	20.9	63.0	81.8	14.0	57.4	78.7

Table 3. Total PET spatial resolution, as assessed by root mean square of the positron range distribution and 3 mm PET camera spatial resolution, according to Eq. <equationcite>3</equationcite>

Radio-nuclide	Compact bone		Soft tissue		Adipose tissue		Lung tissue	
	$FWHM^h_{total}$ (mm)	$FWHM^t_{total}$ (mm)	$FWHM^h_{total}$ (mm)	$FWHM^t_{total}$ (mm)	$FWHM^h_{total}$ (mm)	$FWHM^t_{total}$ (mm)	$FWHM^h_{total}$ (mm)	$FWHM^t_{total}$ (mm)
^{18}F	3.00 (1.3%)	3.03 (~0%)	3.01 (3.2%)	3.05 (1.9%)	3.01 (2.2%)	3.05 (2.2%)	3.02 (17.7%)	3.36 (8.4%)
^{11}C	3.01 (2.6%)	3.06 (~0%)	3.01 (8.2%)	3.15 (3.9%)	3.01 (10.9%)	3.21 (5.0%)	3.04 (30.1%)	4.03 (7.3%)
^{13}N	3.01 (4.14%)	3.08 (~0%)	3.02 (11.2%)	3.25 (4.4%)	3.02 (15.4%)	3.38 (5.3%)	3.06 (36.6%)	4.61 (4.5%)
^{15}O	3.02 (10.4%)	3.19 (5.3%)	3.03 (19.8%)	3.53 (6.6%)	3.04 (23.4%)	3.79 (4.5%)	3.12 (45.8%)	6.09 (5.7%)
^{68}Ga	3.02 (13.2%)	3.27 (6.0%)	3.04 (23.0%)	3.57 (9.6%)	3.05 (25.6%)	4.02 (1.9%)	3.16 (48.0%)	6.79 (11.7%)
^{82}Rb	3.05 (26.3%)	4.02 (2.9%)	3.09 (39.1%)	5.08 (~0%)	3.11 (38.5%)	5.24 (3.4%)	3.32 (58.6%)	10.9 (35.9%)

$FWHM^h$ and $FWHM^t$ represent, respectively, the use of FWHM and FW20M of the positron annihilation distribution in the root mean square calculation. Values within parenthesis are the deviations (%) from FWHM of directly convolved data

contribution of the positron flight to the loss of spatial resolution in the image plane. In a PET camera with 3 mm system resolution, for instance, the loss of spatial resolution due to the positron distance of flight accounts for 1.3% in bone and 3.5% in soft tissue but up to 22.5% in lung tissue for ^{18}F. The corresponding values were, respectively, 2.9%, 9.3% and 45.0% for ^{11}C and 37.9%, 68.9% and 167% for ^{82}Rb.

The results obtained by estimating the total PET spatial resolution using the root mean square method of Eq. 3 are presented in Table 3. Also indicated are the deviations from the FWHM values obtained after direct convolution, $FWHM(T_{j,Z}X^A)_{Convolved}$. From these results, it is shown that the measure of the width at the 20% amplitude level, FW20M, seems to be a more representative measure than FWHM in estimations of the spatial resolution losses due to the positron flight in PET.

Finally, the maximum deviation of the results obtained by changing the sampling energy interval grid from 50 keV to 25 keV in the Monte Carlo calculations was negligible for all tissues and for all radionuclides. Therefore the presented results are consistent with respect to energy rebinning effects.

Discussion

The impact of the positron flight on spatial resolution in PET imaging has often been considered but has generally not been recognised as a major limiting factor for PET spatial resolution. A drawback of most of these investigations is that they have been restricted to positron transport in water. However, the present work revealed large differences in the slowing down of positrons before annihilation for various human tissues. These findings may be of clinical importance, especially in imaging of tumours sited within or at the border of the lungs. In lung tissue, the positron contribution to image blur was found to be up to three times larger than in soft or adipose tissue and five times larger than in bone tissue. Even though tumour masses in the lungs may have a density similar to soft tissue, positrons emitted close to their surface will act to blur the tumour edge and impair their detectability.

In clinical examinations with modern PET cameras, with a spatial resolution between 5 and 7 mm (FWHM) and in sole combination with ^{18}F-labelled compounds, the impact of positron flight on the PET image blur is fairly low in all tissues, with the possible exception of

the lungs. However, as shown by the results in Fig. 3, this situation may change quite drastically with the design and application of ultra-high spatial resolution PET cameras with 3–4 mm spatial resolution in combination with alternative radionuclide-labelled radiopharmaceuticals. The situation is even more critical in the design and use of animal high-resolution PET cameras with a spatial resolution in the order of 1–2 mm. In these cases, the positron flight will be the limiting factor in lung tissue regardless of the choice of radionuclide. For biochemistry and flow investigations in more dense tissues, ^{18}F-labelled substances are to be preferred if the high spatial resolution capacity of these systems is to be fully exploited.

The average range or the FWHM of the positron flight distribution in water has been commonly used as a measure of the spatial resolution losses due to the positron flight distribution in PET. However, as indicated by the results of this work, the projected distribution of annihilation origins around a point source has a shape that differs from a Gaussian distribution. Hence, the conventional measures like FWHM or FWTM of the positron distribution do not accurately predict the spatial resolution losses in PET. Furthermore, a much lower fraction of events are present within the conventional limits for the positron annihilation distribution than for a corresponding Gaussian function. The long tails of the obtained annihilation probability distributions around the positron source are likely to contribute to the image blur with low-frequency components, mixed with those of the scatter distribution. This has to be carefully considered when selecting a single width parameter for estimating the resolution losses according to Eq.3. The full width at twentieth maximum measure, $FW20M(T_{j,Z}X^{A})_{aPSF}$, was found to produce values that were relatively close to those obtained by convolving the annihilation distribution function with the (Gaussian) system resolution function for compact bone, soft tissue and adipose tissue. For lung tissue, the differences remained fairly large and displayed a tendency to increase with increasing positron emission energy.

The relative impact of positron flight on the total spatial resolution in this work was analysed by assuming a Gaussian-shaped system resolution of the PET camera. This Gaussian function comprises the triangular-shaped image blur due to detector size, the non-colinearity of annihilation photons and the parallax errors due to the varying depth of interaction of photons in the detectors. No specific analysis of the individual impact of these factors was made.

As opposed to well-known radiation transport Monte Carlo systems in medical physics, such as EGS4 [17], the PENELOPE Monte Carlo method used in this paper does consider specific positron interactions instead of assuming positrons to behave like electrons. For our specific simulations, the main positron interaction processes were considered to be elastic atomic scattering, inelastic positron-electron scattering and annihilation, although bremsstrahlung was also included. In PENELOPE, these main processes are described by a screened Rutherford restricted differential cross-section, from a first Born approximation obtained from the Sternheimer-Liljequist generalised oscillator strength model and from a Heitler restricted differential cross-section. This, in addition to possible differences in the used positron spectrum distributions for the different radionuclides and in the positron scatter properties between water and soft tissue, might explain the small differences between the spatial resolution data for water, as published by Levin and Hoffman [10], and the corresponding data for soft tissue obtained in this study.

The positron distance of flight represents an unavoidable limiting factor for the PET spatial resolution. Its influence cannot be eliminated by further hardware optimisation; rather this will require new post-processing routines [18], such as shift variant restoration algorithms.

Acknowledgements. We are grateful to Dr Stephen M. Seltzer from the National Institute of Standards and Technology, Gaithersburg, USA, for providing calculated beta energy spectra. This work was funded by the Karolinska Hospital FoUU of the Stockholm Country Council.

References

1. Chatziioannou AF, Cherry SR, Shao Y, Silverman RW, Meadors K, Farquhar TH, Pedarsani M, Pheps ME. Performance evaluation of microPET: a high-resolution lutetium oxyorthosilicate PET scanner for animal imaging. *J Nucl Med* 1999; 40:1164–1175.
2. Melcher Cl. Scintillation crystals for PET. *J Nucl Med* 2000; 41:1051–1055.
3. Brix G, Zaers J, Adam LE, Bellemann ME, Ostertag H, Trojan H, Haberkorn U, Doll J, Oberdoifer F, Lorenz WJ. *Performance evaluation of a whole-body PET scanner using the NEMA protocol.* National Electrical Manufacturers Association. *J Nucl Med* 1997; 38:1614–1623.
4. Adam LE, Karp JS, Daube-Witherspoon ME, Smith RJ. Performance of a whole-body PET scanner using curve-plate NaI(Tl) detectors. *J Nucl Med* 2001; 42:1821–1830.
5. Moses WW, Virador PRG, Derenzo SE, Huesman RH, Budinger TF. Design of a High-resolution, high-sensitivity PET camera for human brains and small animals. *IEEE Trans Nucl Sci* 1997; NS-44:1487–1491.
6. Budinger TH. PET instrumentation: what are the limits? *Semin Nucl Med* 1998; 3:247–267.
7. Derenzo SE. Precision measurement of annihilation point distributions for medically important positron emitters. In: *Positron annihilation.* Sendai, Japan: The Japan Institute of Metals; 1979:819–823.
8. Cho ZH, Chan JK, Eriksson L, Singh M, Graham S, MacDonald NS, Yano Y. Positron ranges obtained from biomedical important positron-emitting radionuclides. *J Nucl Med* 1975; 16: 1174–1176.
9. Palmer MR, Brownell GL Annihilation density distribution calculations for medically important positron emitters. *IEEE Trans Med Imaging* 1993; 11:373–378.

10. Levin CS, Hoffman EJ. Calculation of positron range and its effect on the fundamental limit of positron emission tomography system spatial resolution. *Phys Med Biol* 1999; 44:781–799.
11. Baró J, Sempau J, Férnandez-Varea JM, Salvat F. PENELOPE: an algorithm for Monte Carlo simulation of the penetration and energy loss of electrons and positrons in matter. *Nucl Instrum Meth* 1995; B100:31–46.
12. Sampau J, Acosta E, Baró J, Fernández-Varea JM, Salvat F. An algorithm for Monte Carlo simulation of coupled electron-photon transport. *Nucl Instrum Meth* 1997; B132:377–390.
13. Salvat F, Fernández-Varea JM, Acosta E, Sempau J. PENELOPE, a code system for Monte Carlo simulation of electron and photon transport. OECD/NEA 5–7 November 2001, NEA/NSC/DOC(2001)19. ISBN: 92–64–18475–9
14. ICRU. International Commission on Radiation Units and Measurements. *Photon, electron, proton and neutron interaction data for body tissues.* 1992: Report 46.
15. ICRP. International Commission on Radiological Protection. *Reference man: anatomical, physiological and metabolic characteristics.* ICRP Publication 23. New York: Pergamon Press, 1975.
16. Cross WG, Ing H, Freedman N. A short atlas of beta-ray spectra. *Phys Med Biol* 1983; 28:1251–1260.
17. Bielajew AF, Hirayama H, Nelson WR, Rogers DWO. History, overview and recent improvements of EGS4. Report NRCC/PIRS-0436, June 1994.
18. Haber SF, Derenzo SE, Uber D. Application of mathematical removal of positron range blurring in positron emission tomography. *IEEE Trans Nucl Sci* 1990; NS37:1293–1299.